Iranian Journal of Microbiology
Volume 14 Number 4 (August 2022) 518-528

ORIGINAL ARTICLE

Silver nanoparticles biosynthesis using an airborne fungal isolate, *Aspergillus flavus*: optimization, characterization and antibacterial activity

Aram Al-Soub[1], Khaled Khleifat[2], Amjad Al-Tarawneh[3], Muhamad Al-Limoun[1], Ibrahim Alfarrayeh[1*], Ahmad Al Sarayreh[1], Yaseen Al Qaisi[1], Haitham Qaralleh[4], Moath Alqaraleh[5], Anas Albashaireh[1]

[1]Department of Biological Sciences, Faculty of Science, Mutah University, Al-Karak, Jordan
[2]Department of Medical Laboratory Sciences, Faculty of Allied Medical Sciences, Al-Ahliyya Amman University, Amman, Jordan
[3]Prince Faisal Center for Dead Sea, Environmental and Energy Research, Mutah University, Mutah, Karak, Jordan
[4]Department of Medical Laboratory Sciences, Faculty of Science, Mutah University, Al-Karak, Jordan
[5]Pharmacological and Diagnostic Research Center (PDRC), Faculty of Pharmacy, Al-Ahliyya Amman University, Amman, Jordan

Received: March 2020**, Accepted:** May 2022

ABSTRACT

Background and Objectives: Nanoscience is one of the most important branches of modern science, which deals with the knowledge, structure, and properties of nanoparticles. This study aimed to investigate the ability of an airborne fungus (*Aspergillus flavus*) to synthesize silver nanoparticles (AgNPs) and to test the antibacterial activity of the synthesized AgNPs.

Materials and Methods: The confirmation of AgNPs synthesis and the characterization of their properties were done using UV-Vis spectrophotometer, Zeta potential, Zeta sizer, FT-IR, and XRD analyses. The antibacterial activity was determined using broth microdilution method.

Results: The findings showed that the average diameter of the resultant AgNPs was 474.2 nm with a PDI value of 0.27, and the zeta potential was -33.8 mV. Transmission electron microscopy (TEM) revealed that the AgNPs were regular and spherical in shape. TEM micrographs demonstrated that the AgNPs were smaller than those that were observed by DLS examination because the drying process resulted in particle shrinkage. The average size of AgNPs were less than 35 nm. The AgNPs exhibited a remarkable antibacterial activity against *K. pneumoniae*, *E. coli*, *E. cloacae*, *S. aureus*, *S. epidermidis*, and *Shigella* sp., and the MIC values ranged from 25 to 100 µg/mL. However, an exception was *P. aeruginosa* in which its MIC was >125 µg/mL.

Conclusion: The results suggest that, the biosynthesized AgNPs by *A. flavus* could be utilized as a source of potent antibacterial agents in medicine and biotechnological applications.

Keywords: Nanoparticles; Fungi; Antibacterial agents; Nanomedicine; *Aspergillus flavus*

*Corresponding author: Ibrahim Alfarrayeh, Ph.D, Department of Biological Sciences, Faculty of Science, Mutah University, Al-Karak, Jordan. Tel: +96-2790632435 Fax: +96-2032375540 Email: alfarrayeh@gmail.com

INTRODUCTION

Nanoscience is one of the most important branches of modern science, which deals with the knowledge, structure, and properties of nanoparticles, and at the same time, how these nanoparticles can be applied in all fields of science and technology (1). Therefore, nanoscience and its techniques are considered among the modern and active branches of science, as they are included in many disciplines such as medicine, pharmacy and engineering, and many other fields (2, 3).

Nanoparticles have been described as a group of atoms containing at least one of the three outer dimensions with a size ranging from 1 to 100 nanometers (4, 5). They usually exhibit several unique properties, whether physical or chemical, and of different sizes when matched with their bigger counterparts (6, 7). The unique and new properties have been explored at the nano level and in a wide and varied field of possible applications, whether in medicine, pharmaceuticals, and cosmetics, in renewable energy, polymer industry, environmental treatment, water purification, and in the manufacture of some medical devices (8).

The synthesis of nanoparticles occurs in several ways including chemical, physical and biological methods. Among these methods are chemical methods, with some advantages, to produce them in large quantities and in a short time. However, chemical methods have the disadvantage that they often include the use of toxic materials as helpers and stabilizers, resulting in the production of non-environmentally friendly by-products. On the other hand, physical methods are quick and use radioactive materials as reducing agents without the need for toxic chemicals, but have lower production capacity coupled with high energy consumption, and at the same time lead to unwanted nanoparticle size diversity and contamination of organic solvents (9-11). As a synthetic approach that is environmentally neutral, low cost, safe, uses non-toxic chemicals, and does not contain any harmful by-products, the biological methods are the best. They include intracellular and extracellular methods using bacterial, fungal and plant cells or their extracts collectively called biosynthesis through green nanotechnology (12-14).

Due to their nano size and high surface area, metal nanoparticles exhibit unique and novel physical and chemical properties compared to their macroscale counterparts (15). Silver nanoparticles (AgNPs) are among the metal nanoparticles that have successfully found their way into a variety of products, including soaps, textiles, and plastics (16-18). They are also considered as very interesting and popular antimicrobial agents with a wide spectrum of activities against a variety of pathogenic bacteria and fungi. In the current study, we aimed to optimize and characterize the biosynthesized AgNPs, in addition to the evaluation of their antibacterial activity against various gram-negative and gram-positive bacterial species.

MATERIALS AND METHODS

Fungal strain. The airborne fungus was isolated from the warehouses of the Supplies Department at Mutah University by Dr. Amjad Al-Tarawneh from the Dead Sea Center for Water and Energy at Mutah University, Jordan. The fungal strain was identified to the species level by ITS sequencing as *Aspergillus flavus* (MACROGEN, Korea). After performing a sequence similarity analysis with the NCBI database, the sequence was registered in the NCBI database and the accession number MG973280.1 was obtained.

Preparation of culture conditions for *A. flavus*. The airborne isolate was cultured in the broth media composed of 10 g glucose, 10 g yeast extract, and 5 g NaCl. The growth was maintained for 72 hours at incubation temperature of 33ºC, a pH of 7.0, and a shaking rate of 150 rpm. The cell mass was obtained by filtration using Whatman No. 1 filter paper and washed extensively with deionized distilled water at least four times. The obtained fungal biomass was then used freshly for the preparation of biomass filtrate.

Biosynthesis of AgNPs. The method of Jaidev and Narasimha (19) was adopted for the synthesis of AgNPs with some minor modifications. Briefly, the fungal isolate was grown under aerobic conditions in a liquid culture medium at pH 7.0 by inoculating the liquid medium (100 mL) with 2.0×10^6 spores at 33ºC and 150 rpm for 24 hours. After that, the fungal biomass was obtained by filtration with Whatman No. 1 filter paper and washed thoroughly with sterile and distilled water. Ten grams of wet biomass was placed in 100 ml of sterile deionized water and incubated at

33°C, pH 7.0, and agitated at 150 rpm for 72 hours. Then, the fungal filtrate was obtained by separating the fungal biomass from the suspension using Whatman No. 1 filter paper. In order to accomplish the biosynthesis process, 100 ml of 1 mM $AgNO_3$ was added to the fungal filtrate. After that, the filtrate was incubated at 33°C and 150 rpm in the dark for 24 hours or as needed if otherwise required. To initially characterize the biosynthesized AgNPs, scanning ultraviolet-visible (UV/VIS) light at the range (280-800 nm) was used. The same approach for the control flask was done but without $AgNO_3$.

Optimization of the filtrate biomass for best AgNPs biosynthesis. To get the best conditions for AgNPs biosynthesis, different incubation conditions were investigated. These conditions included the growth biomass (5, 10, 15, and 20 g), the incubation temperature (25, 27, and 33°C), the pH (3, 4, 5, 6, 7, 8 and 9) and the incubation time profile (0, 24, 48, 72, 96, 120, 144 hours). The optimization conditions were used in order so that each criterion is optimized and then the optimizing factor is used in the subsequent parameter study so after these parameters are sequentially optimized (cell mass, temperature, and pH), the incubation time profile is optimized using different lengths of times. Upon completion of each step, the synthesis of AgNPs was monitored by using UV-visible scanning spectroscopy.

Characterization of AgNPs. The absorbance of the resulted brown color that indicates the formation of AgNPs was spectrophotometrically measured using a UV-1800 spectrophotometer (SHIMADZU, Japan). Repeated cycles of centrifugation at 15000 rpm for 20 minutes each (MIKRO 200 R, Hettich, Germany) were used to recover the biosynthesized AgNPs from the reaction solution, which included resuspension in deionized water for washing. Finally, the collected pellets of AgNPs were vacuum dried (VWR 1410 Vacuum Oven, USA). An FEI Versa 3D Dual Beam instrument (FEI, USA) was used to capture TEM images of the prepared AgNPs to determine their size, distribution, and morphology. The crystalline phase of the prepared AgNPs was determined using MAXima-X XRD-7000 (SHIMADZU, Japan). Proteins and other functional groups responsible for AgNPs stability were revealed using Bruker Alpha FTIR spectrometer (Bruker Optics GmbH, Ettlingen, Germany).

Z-potential and Zetasizer distribution by intensity. Particle size distribution and the zeta potential of AgNPs were determined using Zetasizer Nano-ZS90 (Malvern Instruments, UK). The analysis was performed at a scattering angle of 90 at a temperature of 25°C using samples diluted to different intensity concentrations with de-ionized distilled water.

Preparation of bacterial suspension. The culture medium was prepared according to the standards of the Laboratory Standards Institute (20-22). A pure bacterial colony was selected and grown in a sterile nutrient broth overnight at 37°C. Bacterial growth was set at a value of 0.5 McFarland Standard, with the final absorbance being 0.1 at 620 nm.

Assessment of minimal inhibitory concentration (MIC) of AgNPs. The antibacterial activity of AgNPs was tested against seven isolates of clinical bacterial species, including Gram negative (*Escherichia coli*, *Klebsiella pneumonie*, *Enterobacter Cloacae*, *Shigella* sp., *Pseudomonas aeruginosa*) and Gram positive (*Staphylococcus aureus* and *Staphylococcus epidermidis*) species. Minimal inhibitory concentration (MIC) values were determined for each species using the broth microdilution method, which was performed based on the recommended protocol of the National Committee for Clinical Laboratory Standard Institute (20). Chloramphenicol (Cm), Kanamycin (Km), and Ampicillin (Amp) were used as positive controls. MIC was defined as the lowest concentration of the substance needed to inhibit the growth of bacteria (7, 23, 24).

RESULTS

UV–vis absorption spectra (UV–vis). When the fungal filtrate was incubated with silver nitrate ($AgNO_3$), a dark brown color was formed, while control samples remained unchanged during the 24-120 hours' incubation period (Fig. 1A). An intense dark brown color has appeared after 72 hours of adding $AgNO_3$ and then UV-vis absorption spectra (UV-vis) of the fungal filtrate were measured (Fig. 1B). Absorption values were measured at different intervals as well as when using different temperatures and different pH values. The UV-vis spectrum as in Fig. 1B shows the peak of SPR for AgNPs at 401 nm. Usually, the size and shape of AgNPs are reflected in the magnitude of the absorp-

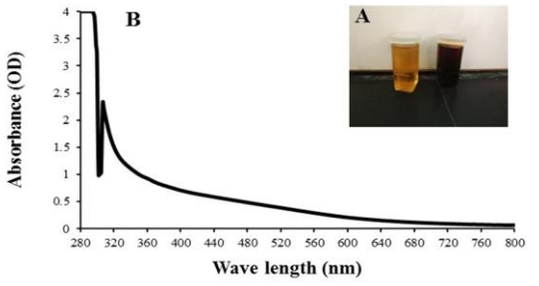

Fig. 1. Solution of 1 mM $AgNO_3$ before and after bioreduction by *A. flavus* prior to the optimization process. Incubation temperature was at 33°C using 10 g biomass, and pH 7, (A) color change and (B) Ultraviolet-Visible spectra.

tion peak (19). The AgNPs were found to be stable in their native form with no observable changes. The biomass filtrate was colorless, thus, indicating that the reduction of the silver ions took place extracellularly likely a result of extracellular nitrate reductase activity produced by the *A. flavus*. Many of the reports on the synthesis of AgNPs by fungi, but this is the first study in which *A. flavus* was used for the possibility of improving the synthesis of AgNPs by studying different parameters of the conditions of the mycelia-containing filtrate.

Effects of biomass on the reduction potential for the filtrate produced by *A. flavus*. The effect of different amounts of biomasses on the biosynthesis of AgNPs was studied by using Uv-vis scanning spectra in the range between 280-800 nm (Fig. 2). The peaked absorbance was 0.835 at 401 nm which was obtained from using the 10 g cell biomass as compared with other weights of cell biomasses tried. Thus, all of the different quantities of cell biomass displayed the formation of AgNPs based on the changes in absorbance measurements at 401 nm, with the 10 g biomass causing the highest amount of AgNPs synthesis.

Effects of incubation temperature of fungal biomass filtrate on the capability of AgNPs biosynthesis. Ten grams of the fungal biomass were suspended in buffered (50 mM phosphate buffer pH 7.0) sterilized deionized water and incubated at 25, 27, and 30ºC and 150 rpm for 72 hours. As the incubation temperature was shifted to 27ºC, there was a significant elevation in AgNPs production (Fig. 3). However, the incubation at 30ºC and 25ºC showed repression of AgNPs synthesis, this is probably due to the inhibition of the enzyme(s) in the fungal filtrate caused by inconvenient incubation temperatures. Further comparison between 25 and 30ºC temperature indicated that the enzyme induction (required for AgNPs biosynthesis) by incubation at 27ºC was obviously significant. A shift in the absorption peak was observed with the change in temperature.

Effect of pH on the reduction potential of *A. flavus* biomass filtrate. Using different pH values of fungal biomass filtrate, the effect of pH variations on AgNPs biosynthesis was investigated (3, 4, 5, 6, 7, 8, and 9). Fig. 4 depicts the effect of pH variation on AgNP biosynthesis. The highest assembly of AgNPs was materialized when the pH of the fungal biomass filtrate was 4. Across the pH ranges tested, the absorption appeared as a shoulder-type peak, but the differences were in the level of absorption, which is reflected by the strength of the brown color in the solution, which in turn reflects the concentration of AgNPs. As part of the evaluation, the absorbance of the $AgNO_3$ -containing biomass filtrate after color change into brown

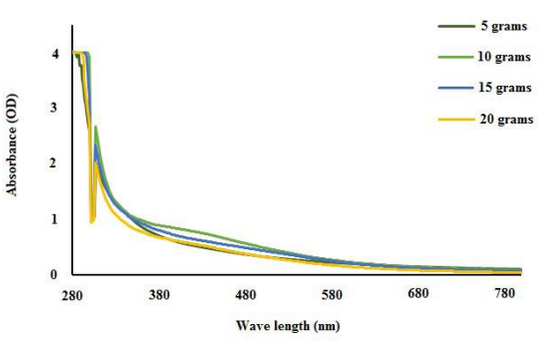

Fig. 2. Effect of fungal biomass weight on the bio-reduction of $AgNO_3$ by mycelia-containing *A. flavus* filtrate.

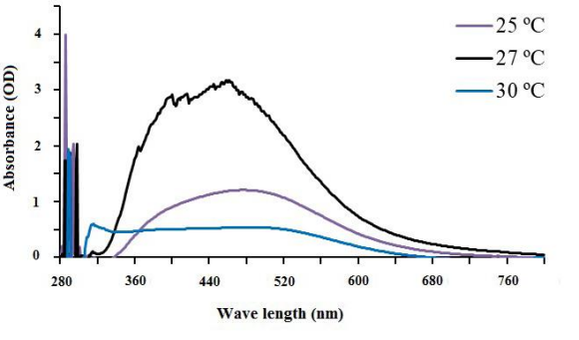

Fig. 3. Effect of incubation temperature on the bioreduction of $AgNO_3$ by mycelia-free culture filtrate as a function of time.

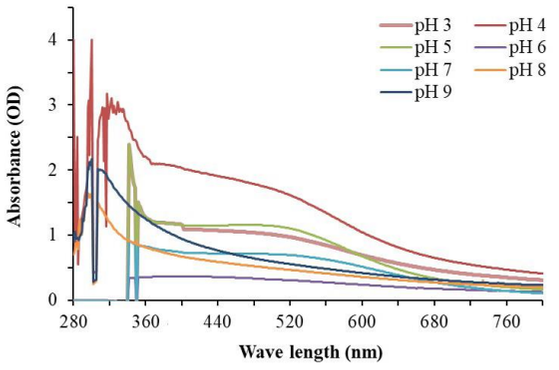

Fig. 4. Effect of pH on bioreduction of $AgNO_3$ by biomass of *A. flavus* -containing filtrate.

was measured. The intensity of the color corresponds to the concentrations of biosynthesized AgNPs. It was observed that when the pH of the fungal biomass filtrate used was 4, a greater amount of AgNPs was formed.

Effect of incubation time on the reduction potential of biomass of *A. flavus* containing filtrate. To obtain optimum incubation periods for the maximum synthesis of nanoparticles, $AgNO_3$ was added to the mycelia-containing culture filtrate having 1.0 mM precursor salt $AgNO_3$ and incubated at 27ºC and pH of 7.0. The length of incubation was 24, 48,72, 96, 120, and 144 hours (Fig. 5). The fungal biomass filtrate reactions were terminated at various time intervals (24, 48. 72, 96, 120, and 144 h). Each sample at its expiry time was taken for the subsequent experiment by adding 0.1 mM silver nitrate to 100 ml of sterile deionized water and left in the incubation as usual for 72 hours, pH 7, and shaking rate of 150 rpm. The AgNPs synthesis for each incubation time

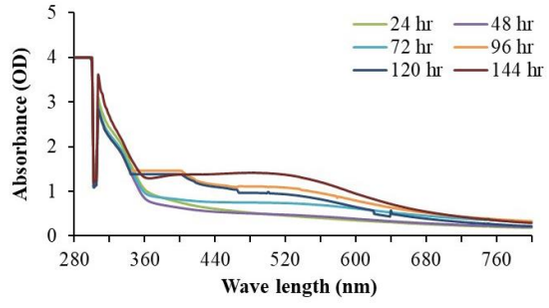

Fig. 5. Effect of incubation time of fungal biomass-containing filtrate on bioreduction of $AgNO_3$ by fungal biomass-free solution as a function of time.

sample was recorded using Uv-vis spectra scanning. Although there was no sign of synthesis at incubation time, zero, the rate of synthesis progressively developed in intensity as a function of reaction time, until the incubation time reached 144 hours beyond which the extent of AgNPs synthesis was unchanged in the sample of 168 hours' time of incubation indicating that, the 144 hours' period of incubation was the best. After completion of the reaction, the AgNPs solution was evidenced for stability as determined by the measurements of UV-vis spectroscopy. It was detected that the nanoparticle solution was unchanging for more than three months, with no signs of aggregation as indicated by ATR-IR results (see below). An interesting Uv-vis spectra peak results for the optimized crude sample were shown at 479 nanometers (Fig. 6A), while when the optimized sample was extensively purified by washing with deionized distilled water, the peak has appeared at 435 nanometers (Fig. 6B).

Characterization of biosynthesized AgNPs: ATR-IR spectrum analysis. The ATR-IR spectrum (Fig. 7) of biologically synthesized AgNPs shows distinct peaks at 3400 cm^{-1} (O-H), 2918 and 2850 cm^{-1} (C-H), 1650 cm^{-1} (C-N and C-C), and 1450 cm^{-1} (vw, N-H and C-N). These groups might be responsible for the synthesis and conformation of the presence of biological systems involved in the biosynthesis of AgNPs.

XRD analysis. The XRD pattern and the presence of peaks confirm the formation of AgNPs nanoparticles by displaying its nature of crystallinity (Fig. 8). The diffracted scans are reordered from $2\theta = 5º$ to 65º. The spectrum appears several Bragg reflections at 27.77º, 32.18º, 38.10º, 46.17º, 54.74º, and 57.69º. The most intense and strong Bragg reflections are 27.77º, 32.18º, and 46.17º. These strong reflections correspond to the crystal planes of (111), (200), (220), and (311), respectively. Generally, the peak at 38.1° is assigned to the (111) planes of the crystalline silver metal particle. This indicates that the process produces a good quality of crystal structure related to AgNPs. The unit cell looks like a cubic crystal structure. A comparison of the obtained XRD spectrum with the standard confirmed that the silver particles formed in the experiments were in the form of nanoparticles in a multi-crystalline form.

Particle size, zeta potential, and morphology. Figs. 9A and B show the probability that there is more

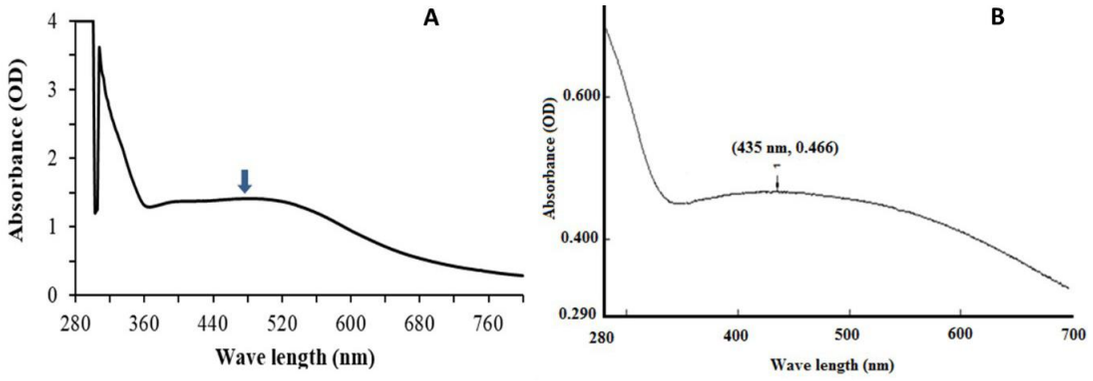

Fig. 6. Solution of 1 mM $AgNO_3$ after bioreduction by *A. flavus* following optimization process of fungal biomass filtrate (fungal biomass containing sterilized distilled water). Incubation temperature was at 27ºC using 10 g biomass, and pH of 4, (A) prior to purification process and (B) after the purification process.

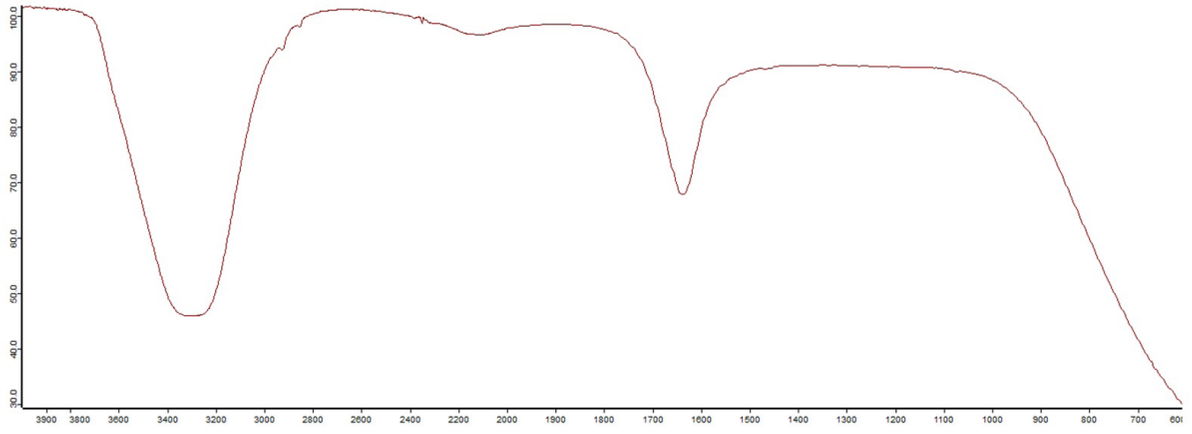

Fig. 7. ATR-IR analysis of biologically synthesized silver nanoparticles.

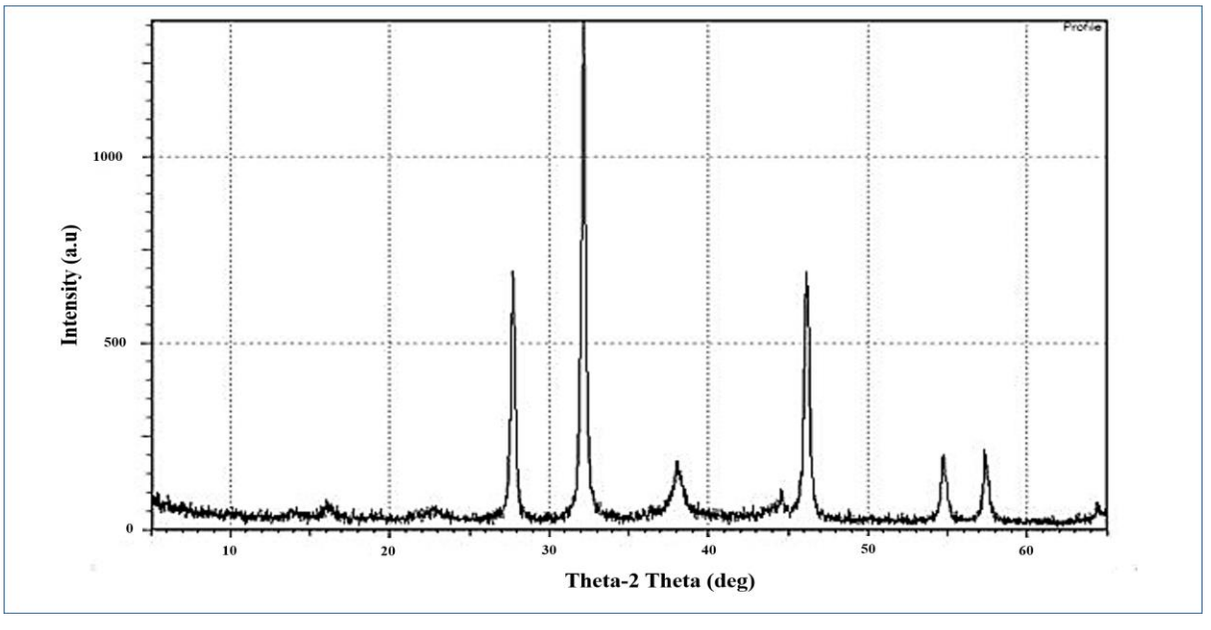

Fig. 8. XRD analysis of biologically synthesized silver nanoparticles.

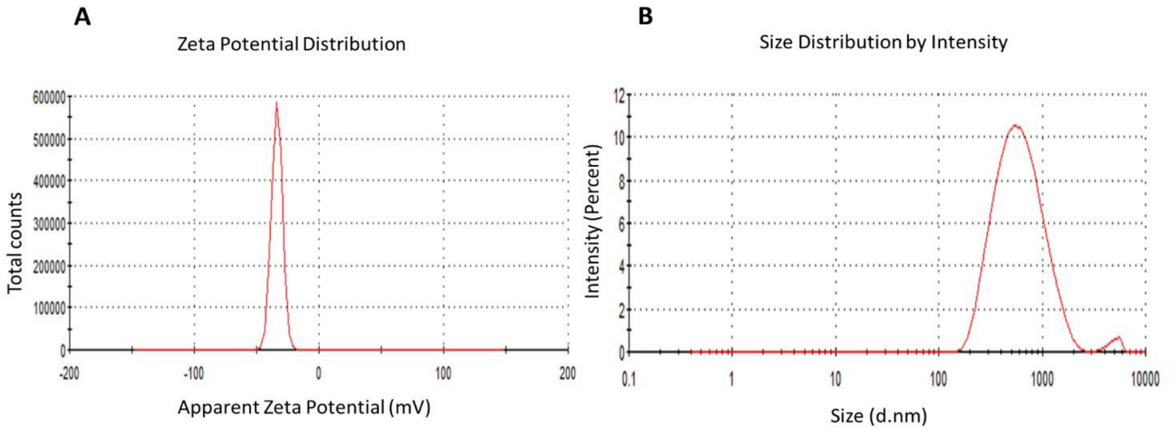

Fig. 9. (A) Zeta potential distribution of silver nanoparticles. AgNPs zeta potential shows – 33.8 mV; (B) The size distribution by the intensity of AgNPs nanoparticles. The size of nanoparticles ranges from 118 to 5000 nm, and the average size is about 474.2 nm.

than one volume present in the sample, so quoting the mean Z in this way may be inappropriate. In our sample, the density distribution shows the relative amount of scattering from groups of various sizes. The particle size distribution obtained from the zeta measurements revealed that the nanoparticle size distribution was found to be 98.01% of the 64.8 nm size of AgNPs. The transmission electron microscope (TEM) images (Fig. 10) shows that the tested particles consist of numerous small objects less than 0.5 µm in size. The TEM image (Fig. 10) shows the displayed nanoparticles with sizes ranging between 10-35 nm and most likely spherical. TEM micrographs demonstrated that the AgNPs were smaller than those that were observed by DLS examination because the drying process resulted in particle shrinkage. The average size of AgNPs was less than 35 nm.

Antibacterial activity of AgNPs. AgNPs exhibited considerable and different levels of antibacterial activity against *K. pneumoniae, E. coli, E. cloacae, S. aureus, S. epidermidis*, and *Shigella* sp. The MIC values were ranging from 25 to 100 µg/mL. However, an exception was *P. aeruginosa* in which the MIC value was above 125 µg/mL (Table 1). The highest antibacterial activity was seen against *E. cloacae* and *K. pneumoniae* followed by *S. epidermidis.*

DISCUSSION

Biological exploration in different and less available conditions has allowed us to study and analyze microbial diversity and confront specialized microbes through the production of biological sourced

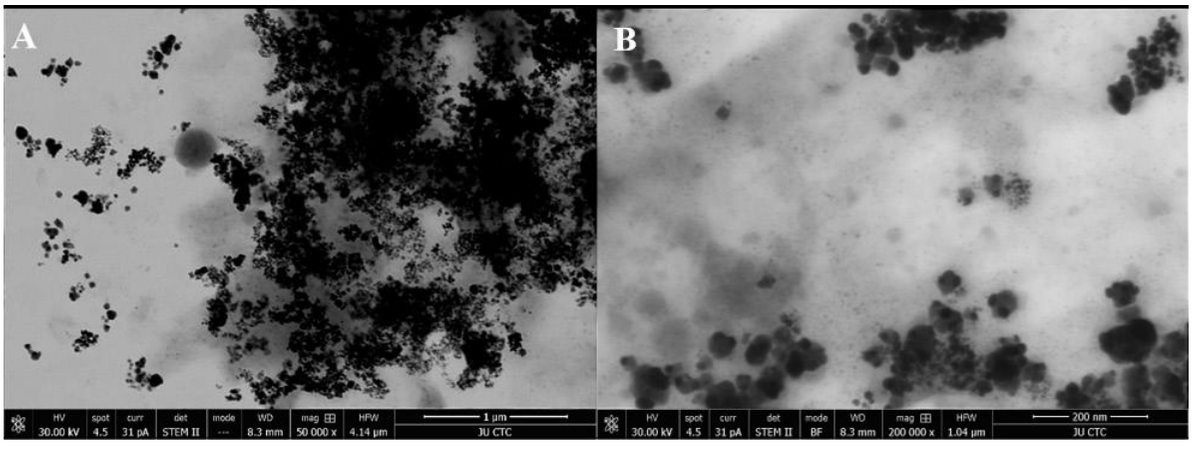

Fig. 10. TEM Image of biosynthesized silver nanoparticles. Magnification (A) 50,000x, (B) 200,000x

Table 1. Minimum Inhibitory concentration of biosynthesized AgNPs and the positive controls against the tested bacteria.

Bacteria	MIC (µg/mL)			
	AgNPs	**Cm**	**Km**	**Amp**
E. coli	75	0.75	0.15	3.0
E. cloacae	25	0.10	0.10	2.0
Shigella sp.	75	0.10	0.15	3.0
P. aeruginosa	> 125	1.0	0.25	5.0
S. epidermidis	50	0.10	0.30	0.25
S. aureus	100	0.25	10.0	0.50
K. pneumoniae	25	0.10	0.50	5.0

compounds, such as metal nanoparticles. When comparing the microorganisms' dependent biosynthesis of AgNPs with chemical and physical methods, the biosynthesis of AgNPs by microorganisms, particularly, fungi is cheaper, more effective and does not involve the use of any risky chemicals (25, 26). In this study, an airborne fungal strain was isolated, identified as *A. flavus*, and registered in the NCBI database with the accession number MG973280.1. This airborne fungal strain revealed its biological ability of being competent for AgNPs biosynthesis. When the fungal filtrate was incubated with silver nitrate ($AgNO_3$), a dark brown color was formed, whereas control samples remained unchanged for the entire 24-120 hours' incubation period. Absorption values were measured at various intervals, as well as at various temperatures and pH levels. The previously detected peak is between 279 and 285 nm for all filtrates without the addition of $AgNO_3$. It is said to be common to biomolecules (27). The main cause of dark brown color formation is attributed to the phenomenon of surface plasmon resonance (SPR) driven by the occurrence of nanoparticles formation. Usually, the size and shape of AgNPs are reflected in the magnitude of the absorption peak (19). The AgNPs were found to be stable in their native form with no observable changes. Two possible mechanisms for the formation of AgNPs by *Fusarium oxysporum* and *Bacillus licheniformis* were reported (19, 28-30); one is through NADH-dependent nitrate reductase and the other by shuttle quinine process (3). The biomass filtrate was colorless, thus, indicating that the reduction of the silver ions took place extracellularly likely a result of extracellular nitrate reductase activity produced by the *A. flavus*. Many of the reports on the synthesis of AgNPs by fungi exist, but this is the first study in which *A. flavus* was used for the possibility of improving the synthesis of AgNPs by studying different parameters of the conditions of the mycelia-containing filtrate.

The optimal fungal biomass used in the formation of the fungal biomass filtrate plays an important role in *A. flavus* cells' ability to produce nanoparticles. Because the peak wavelength at 401 nm did not change significantly, the difference in AgNP concentration can be quantified by tracking the absorption at 401 nm (31). When 10 g of biomass was used, it appeared that the enzyme needed to reduce 1 mM silver nitrate in the optimal incubation time was generated.

Moreover, when the fungal biomass was incubated at different temperatures (25, 27, and 30°C) in a buffered sterilized deionized water (50 mM phosphate buffer, pH 7.0) for 72 hours at 150 rpm, there was a significant increase in AgNPs production at 27°C, which might be the optimal temperature for the enzyme that is responsible for the synthesis AgNPs.

When the pH of the fungal biomass filtrate used was 4 or higher, a greater amount of AgNPs were produced. Nayak et al. reported that if the peak at 420 nm is existent, the nanoparticles are spherical in shape (32). Because the nucleation process for the formation of silver nanocrystals is slow, resulting in a small number of large-size particles, the size of nanoparticles is large at acidic pH. Because –OH ions are easily accessible at high pH, a rapid nucleation process occurs, resulting in the formation of a large number of small particles (33). Obtaining one peak, on the other hand, indicates that the value of the biosynthesized nanoparticles is of high quality. Furthermore, the presence of a shoulder-like peak may indicate the presence of different biological molecules, such as the width and shape of the SPR band, which is reflected in the differentiation of AgNPs formation (34). When the monocular SPR is tight, it reflects the presence of a single diffuse of spherical particles, whereas the wideband reflects the presence of a broad allocation of particles of various sizes (35). The AgNPs synthesis for each incubation time sample was recorded using Uv-vis spectra scanning. The rate of synthesis increased in intensity as a function of reaction time until the incubation time reached 144 hours, after which the extent of AgNPs synthesis was unchanged in the 168-hour sample, indicating that the 144-hour period of incubation was the best. It was detected that the nanoparticle solution was unchanging for more than three months, with no signs

of aggregation as indicated by ATR-IR results. As a result, a capping agent stabilizes the AgNPs particles in solution, which are thought to be proteins secreted into the filtrate by the biomass (36, 37). At 479 nanometers, an interesting UV-vis spectra peak result for the optimized crude sample was shown. However, when the optimized sample was thoroughly purified by washing with deionized distilled water, a peak at 435 nanometers appeared.

The ATR-IR spectrum of biologically synthesized AgNPs shows distinct peaks at 3400 cm^{-1} (O-H), 2918 and 2850 cm^{-1} (C-H), 1650 cm^{-1} (C-N and C-C), and 1450 cm^{-1} (vw, N-H and C-N). These groups might be responsible for the synthesis and conformation of the presence of biological systems involved in the biosynthesis of AgNPs. The XRD pattern and the presence of peaks confirm the formation of AgNPs nanoparticles by displaying its nature of crystallinity. The spectrum appears several Bragg reflections at 27.77°, 32.18°, 38.10°, 46.17°, 54.74°, and 57.69°. The most intense and strong Bragg reflections are 27.77°, 32.18°, and 46.17°. These strong reflections correspond to the crystal planes of (111), (200), (220), and (311), respectively. Generally, the peak at 38.1° is assigned to the (111) planes of the crystalline silver metal particle. This indicates that the process produces a good quality of crystal structure related to AgNPs. The unit cell looks like a cubic crystal structure. A comparison of the obtained XRD spectrum with the standard confirmed that the silver particles formed in the experiments were in the form of nanoparticles in a multi-crystalline form.

The average diameter of the resultant AgNPs was 474.2 nm with a PDI value of 0.27. Accordingly, the PDI (DLS) was higher than 0.2, differentiating a polydisperse distribution (38). The zeta potential was -33.8 mV. Thus, Z values of this size are characteristic of particles that carry a sufficient charge, as they are electrostatically stable and therefore resist self-assembly. The Z-Average is due to the cumulative analysis which gives the hydrodynamic size of the measured auto-conduction function on the principle that the sample may be monodisperse. In the volume density distribution data, show the probability that there is more than one volume present in the sample, so quoting the mean Z in this way may be inappropriate. The density distribution in our sample shows the relative amount of scattering from groups of various sizes. Because light scattering is proportional to particle size, a small amount of a larger component may dominate the gesture. The Number distribution report makes use of the optical properties of the sample to present the relative number based on the size distribution from density distribution data (39). The particle size distribution obtained from the zeta measurements revealed that the nanoparticle size distribution was 98.01 percent of the AgNPs' 64.8 nm size. The transmission electron microscope (TEM) images show that the tested particles are made up of many small objects that are less than 0.5 m in size. However, the structure of the observed AgNPs was difficult to detect because the picture at higher magnification was blurry, which could be attributed to sample charging, the presence of nonconducting carbon stabilizers, and nanoparticle aggregation into larger conglomerates (40). The TEM image of nanoparticles reveals that they are spherical and have sizes ranging from 10-35 nm. TEM micrographs revealed that the AgNPs were smaller than those observed by DLS examination due to particle shrinkage caused by the drying process. The average size of AgNPs was less than 35 nm.

In general, the AgNPs showed a good inhibition with different extents against most bacterial species that were tested. According to our findings, the antibacterial activity of AgNPs was not correlated to the type of bacteria whether Gram-positive or Gram-negative, but it was a species-dependent effect. This is probably due to the differences in the membranes and cell walls of the different bacterial species (41). The highest antibacterial activity was seen against *E. cloacae* and *K. pneumoniae* followed by *S. epidermidis.* On the other hand, *P. aeruginosa* was the most resistant to the AgNPs compared to the other bacterial species, which is in agreement with previous studies (42-45). Thus, AgNPs can be used in any combination with other compounds and through a strategy that minimizes the resistance of bacteria to all kinds of antibiotics (46).

CONCLUSION

The current study highlights the significance of investigated optimization process of AgNPs biosynthesis by airborne fungal biomass containing filtrate. In addition, the promising antibacterial action of the prepared AgNPs against bacterial infections was explored. The results suggest that the biosynthesized AgNPs by *A. flavus* could be utilized as a source of

potent antibacterial agents in healthy medicine and biotechnological application.

ACKNOWLEDGEMENTS

The authors would like to thank the Deanship of Scientific Research at Mutah university/Jordan for supporting this research with grant proposals 315/2020 and 347/2020.

REFERENCES

1. Satalkar P, Elger BS, Shaw DM. Defining nano, nanotechnology and nanomedicine: why should it matter? *Sci Eng Ethics* 2016; 22: 1255-1276.
2. Sergeev GB, Shabatina TI. Cryochemistry of nanometals. *Colloids Surf A Physicochem Eng Asp* 2008; 313-314: 18-22.
3. Qaralleh H, Khleifat KM, Al-Limoun MO, Alzedaneen FY, Al-Tawarah N. Antibacterial and synergistic effect of biosynthesized silver nanoparticles using the fungi Tritirachium oryzae W5H with essential oil of Centaurea damascena to enhance conventional antibiotics activity. *Adv Nat Sci Nanosci Nanotechnol* 2019; 10: 25016.
4. Calderón-Jiménez B, Johnson ME, Montoro Bustos AR, Murphy KE, Winchester MR, Vega Baudrit JR. Silver nanoparticles: Technological advances, societal impacts, and metrological challenges. *Front Chem* 2017; 5: 6.
5. Williams D. The relationship between biomaterials and nanotechnology. *Biomaterials* 2008; 29: 1737-1738.
6. Khleifat K, Alqaraleh M, Al-limoun M, Alfarrayeh I, Khatib R, Qaralleh H, et al. The ability of rhizopus stolonifer MR11 to biosynthesize silver nanoparticles in response to various culture media components and optimization of process parameters required at each stage of biosynthesis. *J Ecol Eng* 2022; 23: 89-100.
7. Alfarrayeh I, Fekete C, Gazdag Z, Papp G. Propolis ethanolic extract has double-face *in vitro* effect on the planktonic growth and biofilm formation of some commercial probiotics. *Saudi J Biol Sci* 2021; 28: 1033-1039.
8. Xu ZP, Zeng QH, Lu GQ, Yu AB. Inorganic nanoparticles as carriers for efficient cellular delivery. *Chem Eng Sci* 2006; 61: 1027-1040.
9. Mafuné F, Kohno JY, Takeda Y, Kondow T, Sawabe H. Formation of gold nanoparticles by laser ablation in aqueous solution of surfactant. *J Phys Chem B* 2001; 105: 5114-5120.
10. Kabashin A V, Meunier M. Synthesis of colloidal nanoparticles during femtosecond laser ablation of gold in water. *J Appl Phys* 2003; 94: 7941-7943.
11. Sylvestre J-P, Kabashin A V, Sacher E, Meunier M, Luong JHT. Stabilization and size control of gold nanoparticles during laser ablation in aqueous cyclodextrins. *J Am Chem Soc* 2004; 126: 7176-7177.
12. Iravani S, Korbekandi H, Mirmohammadi SV, Zolfaghari B. Synthesis of silver nanoparticles: chemical, physical and biological methods. *Res Pharm Sci* 2014; 9: 385-406.
13. Althunibat OY, Qaralleh H, Al-Dalin SYA, Abboud M, Khleifat K, Majali IS, et al. Effect of thymol and carvacrol, the major components of Thymus capitatus on the growth of *Pseudomonas aeruginosa*. *J Pure Appl Microbiol* 2016; 10: 367-374.
14. Alfarrayeh I, Pollák E, Czéh Á, Vida A, Das S, Papp G. Antifungal and anti-biofilm effects of caffeic acid phenethyl ester on different *Candida* species. *Antibiotics (Basel)* 2021; 10: 1359.
15. Gentile A, Ruffino F, Grimaldi MG. Complex-morphology metal-based nanostructures: Fabrication, characterization, and applications. *Nanomaterials (Basel)* 2016; 6: 110.
16. Hossain MK, Drmosh QA, Yamani ZH, Tabet N. (2014). Silver nanoparticles on Zinc Oxide thin film: An insight in fabrication and characterization. In: IOP Conference Series: Materials Science and Engineering. IOP Publishing;. pp. 12018.
17. Fabrega J, Luoma SN, Tyler CR, Galloway TS, Lead JR. Silver nanoparticles: behaviour and effects in the aquatic environment. *Environ Int* 2011; 37: 517-531.
18. Dallas P, Sharma VK, Zboril R. Silver polymeric nanocomposites as advanced antimicrobial agents: classification, synthetic paths, applications, and perspectives. *Adv Colloid Interface Sci* 2011; 166: 119-135.
19. Jaidev LR, Narasimha G. Fungal mediated biosynthesis of silver nanoparticles, characterization and antimicrobial activity. *Colloids Surf B Biointerfaces* 2010; 81: 430-433.
20. CLSI (2012). Methods for Dilution Antimicrobial Susceptibility Tests for Bacteria That Grow Aerobically; Approved Standard—Ninth Edition. CLSI document M07-A9. Wayne, PA: Clinical and Laboratory Standards Institute.
21. Khleifat KM, Tarawneh KA, Ali Wedyan M, Al-Tarawneh AA, Al Sharafa K. Growth kinetics and toxicity of *Enterobacter cloacae* grown on linear alkylbenzene sulfonate as sole carbon source. *Curr Microbiol* 2008; 57: 364-370.
22. Khleifat KM, Sharaf EF, Al-Limoun MO. Biodegradation of 2-Chlorobenzoic acid by *Enterobacter cloacae*: growth kinetics and effect of growth conditions. *Bioremed J* 2015; 19: 207-217.

23. Khleifat K, Abboud M, Al-Shamayleh W, Jiries A, Tarawneh K. Effect of chlorination treatment on gram negative bacterial composition of recycled wastewater. *Pak J Biol Sci* 2006; 9: 1660-1668.
24. Al-Asoufi A, Khlaifat A, Tarawneh AA, Alsharafa K, Al-Limoun M, Khleifat K. Bacterial quality of urinary tract infections in diabetic and non diabetics of the population of Ma'an province, Jordan. *Pak J Biol Sci* 2017; 20: 179-188.
25. Durán N, Durán M, De Jesus MB, Seabra AB, Fávaro WJ, Nakazato G. Silver nanoparticles: A new view on mechanistic aspects on antimicrobial activity. *Nanomedicine* 2016; 12: 789-799.
26. Rahimi R, Ochoa M, Ziaie B. Direct laser writing of porous-carbon/silver nanocomposite for flexible electronics. *ACS Appl Mater Interfaces* 2016; 8: 16907-16913.
27. Gopinath V, Velusamy P. Extracellular biosynthesis of silver nanoparticles using Bacillus sp. GP-23 and evaluation of their antifungal activity towards Fusarium oxysporum. *Spectrochim Acta A Mol Biomol Spectrosc* 2013; 106: 170-174.
28. Durán N, Marcato PD, Alves OL, De Souza GIH, Esposito E. Mechanistic aspects of biosynthesis of silver nanoparticles by several Fusarium oxysporum strains. *J Nanobiotechnology* 2005; 3: 8.
29. Kalimuthu K, Babu RS, Venkataraman D, Bilal M, Gurunathan S. Biosynthesis of silver nanocrystals by Bacillus licheniformis. *Colloids surf B Biointerfaces* 2008; 65: 150-153.
30. Basavaraja S, Balaji SD, Lagashetty A, Rajasab AH, Venkataraman A. Extracellular biosynthesis of silver nanoparticles using the fungus *Fusarium semitectum*. *Mater Res Bull* 2008; 43: 1164-1170.
31. Padalia H, Moteriya P, Chanda S. Green synthesis of silver nanoparticles from marigold flower and its synergistic antimicrobial potential. *Arab J Chem* 2015; 8: 732-741.
32. Nayak RR, Pradhan N, Behera D, Pradhan KM, Mishra S, Sukla LB, et al. Green synthesis of silver nanoparticle by Penicillium purpurogenum NPMF: the process and optimization. *J Nanoparticle Res* 2011; 13: 3129-3137.
33. Chitra K, Annadurai G. Antibacterial activity of pH-dependent biosynthesized silver nanoparticles against clinical pathogen. *Biomed Res Int* 2014; 2014: 725165.
34. Huang J, Zhan G, Zheng B, Sun D, Lu F, Lin Y, et al. Biogenic silver nanoparticles by Cacumen platycladi extract: synthesis, formation mechanism, and antibacterial activity. *Ind Eng Chem Res* 2011; 50: 9095-9106.
35. Riaz M, Mutreja V, Sareen S, Ahmad B, Faheem M, Zahid N, et al. Exceptional antibacterial and cytotoxic potency of monodisperse greener AgNPs prepared under optimized pH and temperature. *Sci Rep* 2021; 11: 2866.
36. Magharbeh M, Al-Hujran T, Al-Jaafreh A, Alfarrayeh I, Sherif E. Phytochemical Screening and in vitro antioxidant and antiurolithic activities of Coffea arabica. *Res J Chem Environ* 2020; 24: 109-114.
37. Alavi M. Bacteria and fungi as major bio-sources to fabricate silver nanoparticles with antibacterial activities. *Expert Rev Anti Infect Ther* 2022; 20: 897-906.
38. Danaei M, Dehghankhold M, Ataei S, Hasanzadeh Davarani F, Javanmard R, Dokhani A, et al. Impact of particle size and polydispersity index on the clinical applications of lipidic nanocarrier systems. *Pharmaceutics* 2018; 10: 57.
39. Cascio C, Geiss O, Franchini F, Ojea-Jimenez I, Rossi F, Gilliland D, et al. Detection, quantification and derivation of number size distribution of silver nanoparticles in antimicrobial consumer products. *J Anal At Spectrom* 2015; 30: 1255-1265.
40. Puchalski M, Dąbrowski P, Olejniczak W, Krukowski P, Kowalczyk P, Polański K. The study of silver nanoparticles by scanning electron microscopy, energy dispersive X-ray analysis and scanning tunnelling microscopy. *Mater Sci* 2007; 25: 473-478.
41. Feng QL, Wu J, Chen GQ, Cui FZ, Kim TN, Kim JO. A mechanistic study of the antibacterial effect of silver ions on *Escherichia coli* and *Staphylococcus aureus. J Biomed Mater Res* 2000; 52: 662-668.
42. Yuan Y-G, Peng Q-L, Gurunathan S. Effects of silver nanoparticles on multiple drug-resistant strains of *Staphylococcus aureus* and *Pseudomonas aeruginosa* from mastitis-infected goats: an alternative approach for antimicrobial therapy. *Int J Mol Sci* 2017; 18: 569.
43. Bhainsa KC, D'souza SF. Extracellular biosynthesis of silver nanoparticles using the fungus *Aspergillus fumigatus. Colloids surf B Biointerfaces* 2006; 47: 160-164.
44. Panáček A, Kvitek L, Prucek R, Kolář M, Večeřová R, Pizúrová N, et al. Silver colloid nanoparticles: synthesis, characterization, and their antibacterial activity. *J Phys Chem B* 2006; 110: 16248-16253.
45. Wu J, Zheng Y, Song W, Luan J, Wen X, Wu Z, et al. In situ synthesis of silver-nanoparticles/bacterial cellulose composites for slow-released antimicrobial wound dressing. *Carbohydr Polym* 2014; 102: 762-771.
46. Chernousova S, Epple M. Silver as antibacterial agent: ion, nanoparticle, and metal. *Angew Chem Int Ed Engl* 2013; 52: 1636-1653.